SUPPLEMENTAL MATERIAL

Fig. S1. ClustalX alignment of Sav1866-dimer vs human SUR1 (in bold).

Fig. S2. A cross-eye stereo view of the 2ONJ.pdb-based $SUR1_{Q1178R}$ core with 2 molecules of the ATP analogue AMP-PNP (the CPK sticks) and 2 Mg^{2+} ions (the gray balls in place of Na^{+} in 2ONJ.pdb). There is no structural template to build the long loop (residues 934-989) connecting the halves of the core. The TMD1-NBD1-half of the core is shown as the lime tube. The TMD2-NBD2-half is shown in cyan tubes, except for the TM15, Coupling, TM16, and TM17 helices, which are shown as ribbons. The R1178 in TM15 is shown in red sticks. Residues within 0.34 nm (the resolution of the template structure) from the R1178 are show in van der Waals spheres (M1251 in TM16; L1294, M1297, V1298, and L1301 in TM17). The conserved 'coupling' or 'transmission' helix (S1,S2) from one half of the core interacts with the nucleotide-bound NBD from the other half of the core, so mutations stabilizing the 'outward-facing' orientation of the last three TM helices from one TMD (for example, TM15, 16, 17) might stabilize the core in its 'open' (stimulatory) conformation with the Mg-nucleotide-bound NBD1/NBD2-dimer. The S1237 (the royal blue vdW spheres) which specifies the sulfonylurea-inhibition of K_{ATP} channels maps to the TM16 helix, not 'a loop' (S3), further indicating the key role of the TM15-16 helical 'transmission-pedal' in the ligand-dependent gating of K_{ATP} channels. We hypothesized that sulfonylurea-binding to the TM16 destabilizes, whereas the R1178 in the TM15 overstabilizes the Mg-nucleotide-bound conformation of the core with the open TM domains; that, respectively, destabilizes and overstabilizes the open state of the K_{ATP} pore. There is no structural template to model the N-terminal portion of SUR1 (TMD0-L0 gatekeeper) that associates with $K_{IR}6.2$ and bidirectionally controls its gating dynamics (S4).

Fig. S3. Currents through single NDSUR1 vs WT K_{ATP} channels in the ligand-free solution, recorded in inside-out patches as described in Experimental Procedures. The mutation does not affect the unitary current amplitude or the ligand-independent activity; the unitary conductance, P_{Omax}, mean open, fast closed, burst, and interburst times at the burst criterion of 2 ms were 74±3 vs 74±2 pS, 0.646±0.051 vs 0.671±0.042, 2.99±0.31 vs 3.01±0.27, 0.29±0.03 vs 0.28±0.04, 119.42±23.72 vs 124.83±25.35, and 49.11±6.48 vs 45.14±5.82 ms for 6 NDSUR1 vs 6 WT channels, respectively.

Table S1. Concatemeric K_{ATP} channels with all possible numbers of NDSUR1 vs SUR1 subunits show similar ligand-independent activity. The activities of the concatemeric K_{ATP} channels were independent of whether $K_{IR}6.2$ subunits were from one or more concatemer(s) or how many receptors of the same kind were from concatemer(s) because SUR1-$K_{IR}6.2$-$K_{IR}6.2$-$K_{IR}6.2$-$K_{IR}6.2$/$SUR1_3$ vs (SUR1-$K_{IR}6.2$-$K_{IR}6.2$)$_2$/$SUR1_2$ vs (SUR1-$K_{IR}6.2$)$_4$ vs $K_{IR}6.2$-$K_{IR}6.2$-$K_{IR}6.2$-$K_{IR}6.2$/$SUR1_4$ vs ($K_{IR}6.2$-$K_{IR}6.2$)$_2$/$SUR1_4$ channels were similarly active, and (SUR1-$K_{IR}6.2$-$K_{IR}6.2$)$_2$/$NDSUR1_2$ vs (NDSUR1-$K_{IR}6.2$-$K_{IR}6.2$)$_2$/$SUR1_2$ channels were undistinguishable. Sixteen single-channel records from heterozygous cells expressing non-concatenated NDSUR1, SUR1, and $K_{IR}6.2$ showed similar *i*, the WT channel-like P_{Omax}, and similar response to 10 μM ATP (>50% inhibition), but at least three dissimilar P_O in millimolar MgATP (differing >2.5-fold from each other), suggesting that the randomly interacting monomeric subunits readily form K_{ATP} species containing both receptors and that 'intermediate' hyperstimulation of concatemeric channels containing both receptors (Fig. 2A,B) is physiologically relevant.

Channel	Mean open time (ms)	Mean fast closed time (ms)	Mean burst duration (ms)	Mean interburst interval (ms)	P_{Omax}
SUR1-($K_{IR}6.2$)$_4$/$SUR1_3$	3.04 ± 0.31	0.28 ± 0.03	375.51 ± 42.28	22.21 ± 3.37	0.865 ± 0.018
NDSUR1-($K_{IR}6.2$)$_4$/$SUR1_3$	3.06 ± 0.29	0.28 ± 0.03	380.34 ± 36.26	24.22 ± 4.02	0.862 ± 0.021
[SUR1-($K_{IR}6.2$)$_2$]$_2$/$NDSUR1_2$	3.05 ± 0.28	0.27 ± 0.02	372.79 ± 31.29	25.05 ± 3.88	0.861 ± 0.017
SUR1-($K_{IR}6.2$)$_4$/$NDSUR1_3$	3.04 ± 0.26	0.27 ± 0.03	401.96 ± 35.44	28.02 ± 4.11	0.858 ± 0.019
NDSUR1-($K_{IR}6.2$)$_4$/$NDSUR1_3$	3.01 ± 0.29	0.29 ± 0.03	360.37 ± 20.35	20.86 ± 4.07	0.863 ± 0.022

References

S1. Dawson, R. J., and Locher, K. P. (2006) *Nature* **443**, 180-185

S2. Dawson, R. J., and Locher, K. P. (2007) *FEBS Lett* **581**, 935-938

S3. Ashfield, R., Gribble, F. M., Ashcroft, S. J., and Ashcroft, F. M. (1999) *Diabetes* **48**, 1341-1347

S4. Babenko, A. P., and Bryan, J. (2003) *J Biol Chem* **278**, 41577-41580

Fig. S1

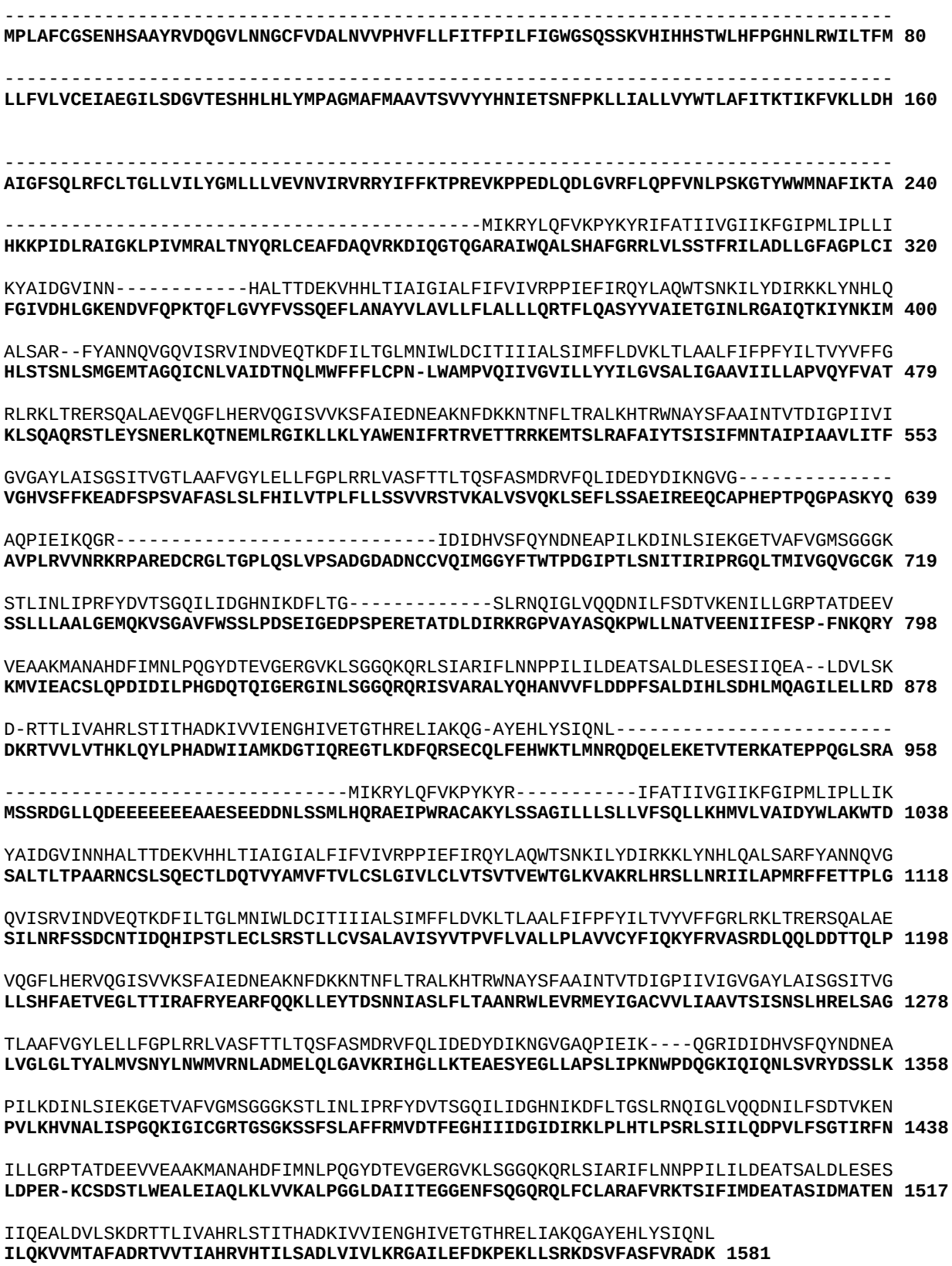
MPLAFCGSENHSAAYRVDQGVLNNGCFVDALNVVPHVFLLFITFPILFIGWGSQSSKVHIHHSTWLHFPGHNLRWILTFM 80
LLFVLVCEIAEGILSDGVTESHHLHLYMPAGMAFMAAVTSVVYYHNIETSNFPKLLIALLVYWTLAFITKTIKFVKLLDH 160
AIGFSQLRFCLTGLLVILYGMLLLVEVNVIRVRRYIFFKTPREVKPPEDLQDLGVRFLQPFVNLPSKGTYWWMNAFIKTA 240
HKKPIDLRAIGKLPIVMRALTNYQRLCEAFDAQVRKDIQGTQGARAIWQALSHAFGRRLVLSSTFRILADLLGFAGPLCI 320
FGIVDHLGKENDVFQPKTQFLGVYFVSSQEFLANAYVLAVLLFLALLLQRTFLQASYYVAIETGINLRGAIQTKIYNKIM 400
HLSTSNLSMGEMTAGQICNLVAIDTNQLMWFFFLCPN-LWAMPVQIIVGVILLYYILGVSALIGAAVIILLAPVQYFVAT 479
KLSQAQRSTLEYSNERLKQTNEMLRGIKLLKLYAWENIFRTRVETTRRKEMTSLRAFAIYTSISIFMNTAIPIAAVLITF 553
VGHVSFFKEADFSPSVAFASLSLFHILVTPLFLLSSVVRSTVKALVSVQKLSEFLSSAEIREEQCAPHEPTPQGPASKYQ 639
AVPLRVVNRKRPAREDCRGLTGPLQSLVPSADGDADNCCVQIMGGYFTWTPDGIPTLSNITIRIPRGQLTMIVGQVGCGK 719
SSLLLAALGEMQKVSGAVFWSSLPDSEIGEDPSPERETATDLDIRKRGPVAYASQKPWLLNATVEENIIFESP-FNKQRY 798
KMVIEACSLQPDIDILPHGDQTQIGERGINLSGGQRQRISVARALYQHANVVFLDDPFSALDIHLSDHLMQAGILELLRD 878
DKRTVVLVTHKLQYLPHADWIIAMKDGTIQREGTLKDFQRSECQLFEHWKTLMNRQDQELEKETVTERKATEPPQGLSRA 958
MSSRDGLLQDEEEEEEEAAESEEDDNLSSMLHQRAEIPWRACAKYLSSAGILLLSLLVFSQLLKHMVLVAIDYWLAKWTD 1038
SALTLTPAARNCSLSQECTLDQTVYAMVFTVLCSLGIVLCLVTSVTVEWTGLKVAKRLHRSLLNRIILAPMRFFETTPLG 1118
SILNRFSSDCNTIDQHIPSTLECLSRSTLLCVSALAVISYVTPVFLVALLPLAVVCYFIQKYFRVASRDLQQLDDTTQLP 1198
LLSHFAETVEGLTTIRAFRYEARFQQKLLEYTDSNNIASLFLTAANRWLEVRMEYIGACVVLIAAVTSISNSLHRELSAG 1278
LVGLGLTYALMVSNYLNWMVRNLADMELQLGAVKRIHGLLKTEAESYEGLLAPSLIPKNWPDQGKIQIQNLSVRYDSSLK 1358
PVLKHVNALISPGQKIGICGRTGSGKSSFSLAFFRMVDTFEGHIIIDGIDIRKLPLHTLPSRLSIILQDPVLFSGTIRFN 1438
LDPER-KCSDSTLWEALEIAQLKLVVKALPGGLDAIITEGGENFSQGQRQLFCLARAFVRKTSIFIMDEATASIDMATEN 1517
ILQKVVMTAFADRTVVTIAHRVHTILSADLVIVLKRGAILEFDKPEKLLSRKDSVFASFVRADK 1581

Fig. S2

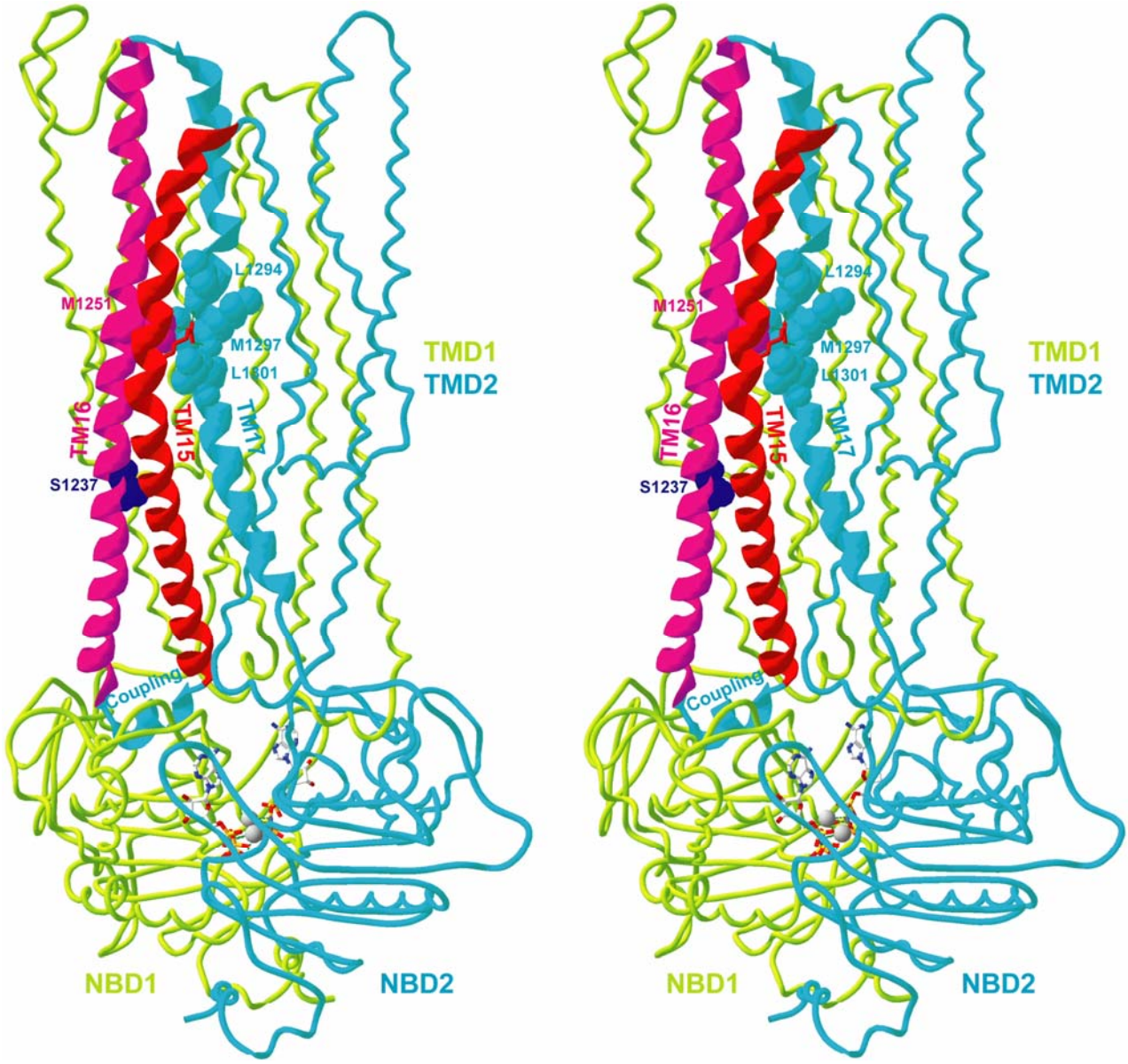
L1294
M1251
M1297
L1301
TMD1
TMD2
TM16
TM15
TM11
S1237
Coupling
NBD1
NBD2
L1294
M1251
M1297
L1301
TMD1
TMD2
TM16
TM15
TM17
S1237
Coupling
NBD1
NBD2

Fig. S3